Preparation and characterization of polyaniline/cerium dioxide (CeO$_2$) nanocomposite via in situ polymerization

E. Kumar · P. Selvarajan · D. Muthuraj

Abstract Crystalline ceria (CeO$_2$) nanoparticles have been successfully synthesized by a microwave-assisted solution method. Polyaniline (PANI)/cerium dioxide (CeO$_2$) nanocomposite was synthesized by in situ polymerization of aniline in the presence of CeO$_2$ nanoparticles. Characterization of CeO$_2$ and PANI/CeO$_2$ nanomaterials are carried out using various studies such as powder X-ray diffraction, infrared spectral and UV–Vis absorption spectral analyses, scanning electron microscopic and high-resolution transmission electron microscopic (HRTEM) studies and thermal analysis. The HRTEM of the images indicate that the CeO$_2$ nanoparticles were embedded in the PANI matrix forming the core–shell structure.

Introduction

Conducting electro-active polymers have attracted considerable attention in recent years because of their potential applications in new technologies such as electrochemical displays, sensors, catalysis, redox capacitors, antistatic coatings, electromagnetic shielding, optical, photoelectrical properties, and secondary batteries [1, 2] and these polymers are usually used to prepare organic–inorganic hybrid materials due to their good stability and controllable thickness and they can be chemically bonded to inorganic materials by method of polysorption. This method is limited to inorganic materials that have active groups (such as hydroxyl group) on their surface [3–5]. Among organic conducting polymers, polyaniline (PANI) has attracted intense interest because of its high conductivity, excellent stability, and relatively high transparency to visible light. These properties make it one of the most applied conducting polymers [6]. For application in optoelectronics, normally the polymeric matrices are the most desirous as the film of the nanoparticles/polymer composite can be cast easily and thus offer direct use in devices. The re-dispersed nanoparticles when loaded in polymer by dissolution of the as-synthesized particles cannot be guaranteed and this leads to difficulties in knowing the concentration of nanoparticles within the polymer. If the nanoparticles are synthesized in polymeric reaction medium, such issues can be tackled with much ease [7]. The use of polymers is a prominent method for the synthesis of nanoparticles. The reason for using the polymers to prepare nanocomposite is to control the growth and morphology of the nanoparticles. Inorganic nanoparticles stand for a class of new materials having enormous applications in broad fields. To obtain the materials with synergetic or complementary behavior between polymer and inorganic nanoparticles, various composites of polymer with inorganic nanoparticles have been synthesized in recent years [8–13]. Among those inorganic nanoparticles, cerium dioxide (CeO$_2$) nanoparticles have been intensively studied due to their unique catalytic, electrical, and optic properties, as well as their extensive applications in diverse areas [14–19]. A variety of methods such as co-precipitation, hydrothermal,

E. Kumar (✉)
Department of Physics, Infant Jesus College of Engineering and Technology, KeelaVallanadu,
Tuticorin 628 851, Tamilnadu, India
e-mail: kumarnano@gmail.com

P. Selvarajan
Department of Physics, Aditanar College of Arts and Science,
Tiruchendur 628 216, Tamilnadu, India

D. Muthuraj
Department of Physics, The M.D.T Hindu College,
Tirunelveli 627 010, Tamilnadu, India

sol–gel method, microemulsion method etc. based on wet chemical routes have been extensively employed to synthesize of ceria (CeO_2) nanoparticles [20–24]. In this study, ceria nanoparticles were synthesized by microwave-assisted solution method. PANI/CeO_2 nanocomposite is synthesized by in situ polymerization of aniline in the presence of CeO_2 nanoparticles and the prepared pure ceria nanoparticles and PANI/CeO_2 nanocomposite were characterized by various studies.

Experimental

Materials

The aniline (AR grade MERCK) was distilled twice under reduced pressure. Ammonium persulphate (APS) [$(NH_4)_2 S_2O_8$] (Analytical reagent, RANBAXY fine chemicals Limited, India), hydrochloric acid (AR grade MERCK) and ammonium Ce(IV) nitrate, [$(NH_4)_2Ce(NO_3)_6$] (AR grade MERCK) and sodium hydroxide (NaOH) (AR grade MERCK) were used to prepare the nanocomposites of this study. Water used in this investigation was de-ionized water.

Synthesis

Synthesis of CeO_2 nanoparticles

Initially, ceria (CeO_2) nanoparticles were prepared as follows: the precursors like ammonium Ce(IV) nitrate and sodium hydroxide (NaOH) were taken in 1:4 molar ratio and dissolved completely in de-ionized water. Here, the pH value of the solution was adjusted to be 12. The mixture solution was stirred well using a magnetic stirrer for about 1 h with a stirring rate of 1000 rpm. Then the prepared mixture solution was kept in the microwave oven (900 W, 2450 MHz, Onida, India) at a temperature of 50 °C for about 30 min. When ammonium ceric nitrate is treated with sodium hydroxide, the hydrolysis process took place and the products like sodium nitrate, ammonium hydroxide, and cerium hydroxide were formed. During the reaction, one proton (H^+) is removed from cerium hydroxide due to polar nature of water and this lead to the formation of hydrated CeO_2. Synthesized pale-yellow precipitate was filtered and washed with de-ionized water twice. Annealing of the synthesized powder at 130 °C in air for 2 h will result in the formation of CeO_2 nanoparticles.

Synthesis of PANI/CeO_2 nanocomposite

PANI/CeO_2 nanocomposite was prepared as follows: 4.5 ml aniline was injected into 70 ml of 2 M of HCl containing 2 g of CeO_2 nanoparticles under ultrasonic action to reduce the aggregation of nanoparticles. After 12 h, 4.5 g of APS was dissolved in 20 ml de-ionized water and it was dropped into solution with constant stirring for about 10 min. The polymerization was allowed to proceed for 3 h at 30 °C. Reaction mixture was filtered under gravity, and washed with 2 M HCl and de-ionized water, afterward dried at 90 °C for 12 h in vacuum to obtain a fine tint green powder.

Instrumentation

Powder X-ray diffraction (XRD) pattern of the nanoparticles were obtained using a powder X-ray diffractometer (PANalytical Model, Nickel filtered Cu Kα radiations with $\lambda = 1.54056$ Å at 35 kV, 10 mA). The sample was scanned over the required range for 2θ values (10°–70°). The FT-IR spectrum of the sample was recorded using a Shimadzu 8400S spectrometer by the KBr pellet technique in the range 400–4500 cm^{-1}. The optical spectra of nanocomposites have been recorded in the region 190–1100 nm using a UV-1800 series spectrophotometer in the absorption mode. TG/DTA of the nanoparticles of this study were carried out simultaneously using Seiko thermal analyzer in air atmosphere at a heating rate of 20 °C/min for a temperature range of 20–1000 °C. The alumina crucible was used. The scanning electron microscopic (SEM) image of the synthesized CeO_2 nanoparticles was recorded using a Hitachi Scanning Electron Microscope. The size and shape of nanoparticles were obtained by high-resolution transmission electron microscope (HRTEM) and the measurements were carried out on a JOEL JEM 2000.

Results and discussion

Structural characterization

XRD studies

The powder XRD pattern for the as-prepared pure CeO_2 nanoparticles is presented in the Fig. 1a. It was observed that the XRD reflection peaks for pure CeO_2 sample and was in a perfect match with the diffraction pattern of CeO_2 published in the (JCPDS File No. 34-0394). All the reflections of powder XRD patterns of this study are indexed using the TREOR and INDEXING software packages. The exhibited XRD peaks corresponded to the (1 1 1), (2 0 0), (2 2 0), (3 1 1), (2 2 2), (4 0 0), (3 3 1), and (4 2 0) of a cubic fluorite structure of CeO_2 and it is identified using the standard data [25, 26]. The obtained values in this study are in good agreement with the values reported by other research group [27–29]. The unit cell parameters of the sample are found

using the software "UNITCELL" and the observed values are $a = b = c = 5.407$ Å and $\alpha = \beta = \gamma = 90°$. The powder XRD pattern of CeO_2 nanoparticles had shown broad peaks, which confirmed the formation of small-sized nanoparticles. The particle size of nanoparticles are determined using the Scherrer's relation $d = (0.9\lambda)/(\beta\cos\theta)$, where β is the full width at half maximum in radians, λ is the wavelength of X-rays used, and θ is the Bragg's angle [30]. For the various reflection peaks of the XRD pattern, the particle size is estimated and the average size of nanoparticles of the sample is found to be around 20 nm.

The XRD pattern of pure PANI synthesized in this study is presented in Fig. 1b. It has shown that PANI has partly crystalline structure and the intense peak at $2\theta = 25.3°$ has a similar profile as that of pure PANI reported in literatures [31, 32]. The PANI nanomaterial displayed in a broad peak at 2θ ranging from 15° to 30° is reported as the characteristic distance between the ring planes of benzene ring in adjacent chain. The broad peak of PANI due to the ring planes of benzene is noticed as a higher background in the region 18°–35° and it also has some degree of crystallinity. A maximum peak, which is around 25° for PANI, should be assigned to the scattering from the periodicity perpendicular to PANI chains [33].

Figure 1c has presented the XRD pattern of PANI/CeO_2 nanocomposite and it shows the characteristic peaks not only for the PANI but also for the CeO_2 nanoparticles, proving that the existence of CeO_2 nanoparticles within the composites, whereas the peaks related to the CeO_2 nanoparticles centered at $2\theta = 28.5°$, 33.6°, 47°, and 58° had become more sharp and crystalline. This confirms that the PANI/CeO_2 nanocomposite has become more crystalline as the concentration of CeO_2 is increased and PANI deposited on the surface of CeO_2 nanoparticles has no effect on the crystallization behavior of CeO_2 nanoparticles in the nanocomposite [34]. In PANI/CeO_2 nanocomposite, the observed diffraction lines are indexed to ceria nanoparticles and it had agreed well with the JCPDS ICDD card no. 34-0394. The observed broad and sharp peaks corresponding to those of PANI and CeO_2 has indicated that there is no structural change but only conformational change in the polymer backbone due to the addition of CeO_2. The low angle peak which is observed in PANI is also present in Fig. 1b but it was sharp due to the overlapping of CeO_2 peak and it can be seen that the XRD pattern of the nanocomposite contains contributions from both the PANI and the CeO_2 nanoparticles. However, a maximum peak centered at $2\theta = 28.556°$ in the CeO_2 nanoparticles has shifted to $2\theta = 25.3°$, and some peaks of the CeO_2 nanoparticles is disappeared in the PANI/CeO_2 nanocomposite. Through this we could find that the polymerization of aniline on the surface of CeO_2 nanoparticles causes no crystalline change of CeO_2 nanoparticles. The

crystallite size (D) is calculated using the Scherrer's formula and is found to be between 10 and 20 nm.

FT-IR spectral analysis

The infrared spectroscopy is effectively used to identify the functional groups of the synthesized compounds. The FT-IR spectrum of the nanoparticles of CeO_2 is shown in Fig. 1d. The broad absorption band located around 3448 cm^{-1} corresponds to the O–H stretching vibration of residual water and hydroxyl groups, while the absorption band at 1647 cm^{-1} is due to the scissor bending mode of associated water. The bands at 2939.3 and 2453.3 cm^{-1} are corresponding to C–CH_2 asymmetric stretching vibration and C–CH_2 symmetric stretching vibration, respectively. The bands at 3382.9 and 1647.1 cm^{-1} can be attributed to the O–H vibration in absorbed water on the sample surface [28]. In addition to the bands in 850–1600 and 2800–3000 cm^{-1}, the band due to the stretching frequency of Ce–O can be seen below 700 cm^{-1}. The FT-IR peaks at about 1515, 1265, 1130, 1064, 952, and 862 cm^{-1} are similar to those of commercial CeO_2 powders [35] and CeO_2 nanoparticles [36]. The bands at 862 and 819 cm^{-1} corresponds to (Ce–O) metal–oxygen bond and the assignments for the peaks/bands of the FT-IR spectra of the samples have been given in accordance with the data reported in the literature [37].

The FT-IR spectrum of the PANI/CeO_2 nanocomposite is shown in Fig. 1e. From the results, it is observed that FT-IR spectra of PANI/CeO_2 nanocomposites contain contributions from both the CeO_2 nanoparticles and the PANI. However, some bands of PANI had shifted due to interactions with CeO_2 nanoparticles. For example, the bands at 1556, 1477, and 1299 cm^{-1}, corresponding to the stretching mode of C–N, C–C, and C–N, all shifted to lower wavenumbers 1554, 1471, and 1298 cm^{-1}, and N–H stretching band at 3465 cm^{-1} shifted to lower wavenumber. Similarly, the band at 1116 cm^{-1} has shifted to 1122 cm^{-1}. The peak at 810 cm^{-1} also shifted to 802 cm^{-1}, attributed to an aromatic C–H out-of-plane deformation vibration of the para disubstituted benzene ring. These changes suggested that C–N, C–C, and C–N bands became stronger in PANI/CeO_2 nanocomposite, but the N–H band became weaker. This was probably because of the action of hydrogen bonding between the surfaces of CeO_2 nanoparticles and the N–H groups in PANI macromolecules. The change in intensity of the IR spectra is believed to the fact that, because of the presence of CeO_2 particles in the reaction system, aniline gets adsorbed on the oxide particles. Polymerization proceeds initially on the surface of these oxide particles when $(NH_4)_2 S_2O_8$ is added to the reaction system. The adsorption of polymer to the CeO_2 nanoparticles results in constrained chain growth
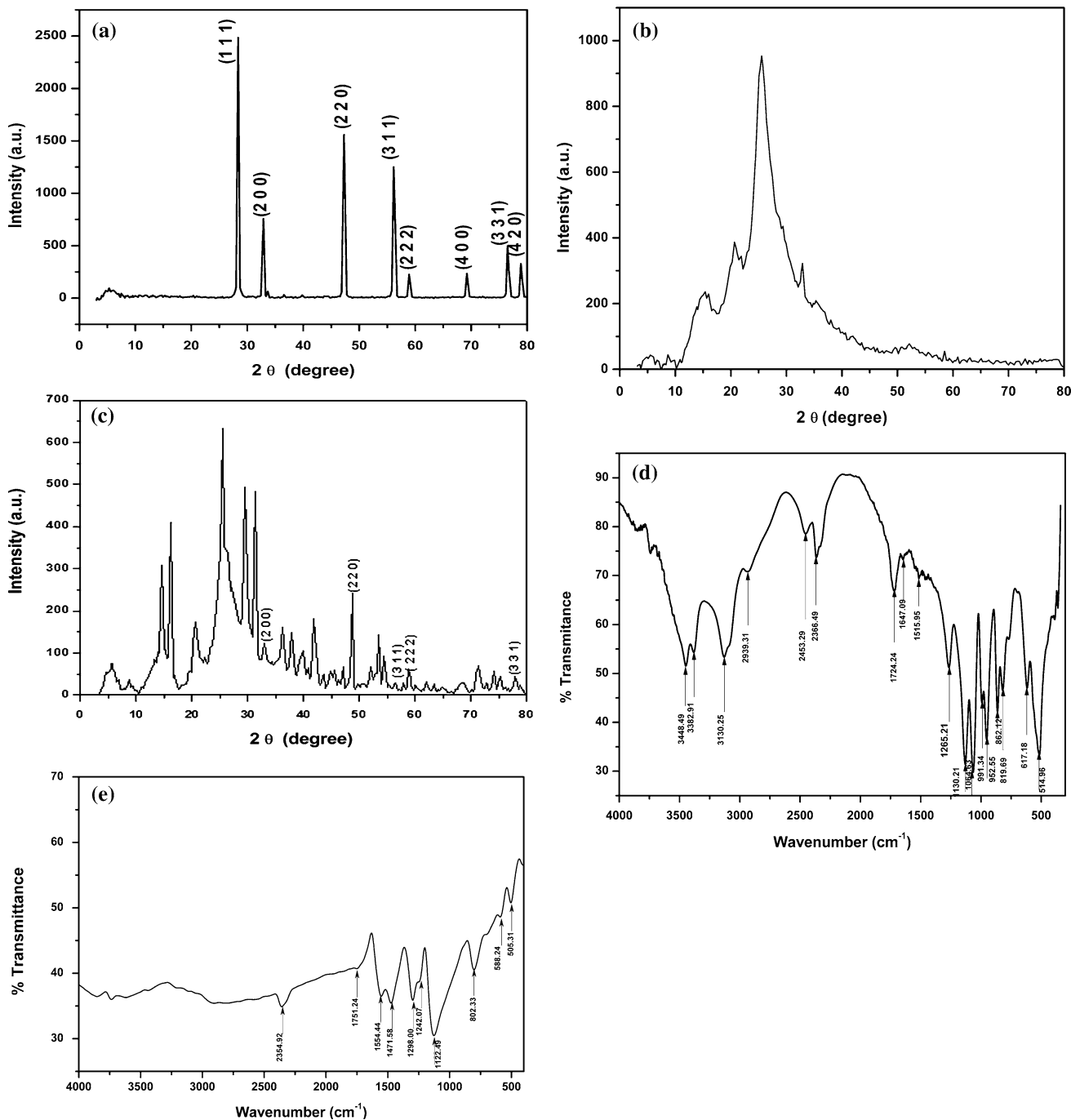
Fig. 1 **a** XRD powder pattern of CeO_2 nanoparticles. **b** XRD pattern of PANI. **c** PANI/CeO_2 nanocomposite. **d** FT-IR spectra of CeO_2 nanoparticles. **e** PANI/CeO_2 nanocomposite

around the nanoparticles. Such adsorption and constrained motion of the chains will restrict the modes of vibration in PANI, which in turn leads to the change in intensity in the IR spectra [33]. In the PANI/CeO_2 nanocomposite, the bands at 588 and 505 cm^{-1} are attributed to the CeO_2 nanoparticles. The assignments for the peaks/bands of the FT-IR spectra of the samples have been given in accordance with the data reported in the literature [38].

UV–Visible spectral analysis

UV–Visible absorption spectral study may be assisted in understanding electronic structure of the optical band gap of the material. Absorption in the near ultraviolet region arises from electronic transitions associated within the sample. UV–Visible absorption spectra of pure CeO_2 nanoparticles and PANI/CeO_2 nanocomposite dispersed in

ethanol solution were recorded and they are presented in Fig. 2a and b. Figure 2a shows a well-defined absorption peak located at 321 nm. The sharp and strong absorption spectrum with clear excitonic feature is in good accordance with the narrow size distribution of ceria nanocrystal. In comparison with UV–Visible absorption spectrum of CeO_2 nanoparticles reported in the literature [39], the peaks at 321 nm and band/peak in the spectrum located at around 500–700 nm are observed to be shifted toward lower wavelength side, which clearly shows the blue shift. It indicates that the absorption positions depend on the morphologies and sizes of CeO_2.

Figure 2b shows the optical absorption spectrum of PANI/CeO_2 nanocomposite and it exhibits a sharp peak at 324 nm and shoulders at 648 and 848 nm. The peak at 324 nm corresponds to the π–π^* transition of the benzenoid rings, while the shoulder at 648 nm corresponds to the polaron absorption band. However, the increasing absorption of small peak at 848 nm is assigned to the conducting emeraldine salt phase of the polymer. Localized polaron bands at around 648 and 848 nm are characteristic peaks of emeraldine salt of PANI [40, 41]. On comparison with UV–Vis absorption spectrum of pure PANI with that of nanocomposite, there is not much variation observed, except the formation of polaronic peak at 273 nm in the spectrum of nanocomposites which is absent in the pure PANI spectrum. Notable differences in the spectra were observed in the formation of different oxidation states as well as for their positions and intensities with respect to the CeO_2 nanoparticles used. Thus, from the optical spectroscopy it is observed that the size and nature of the dopant ions plays an important role in the formation
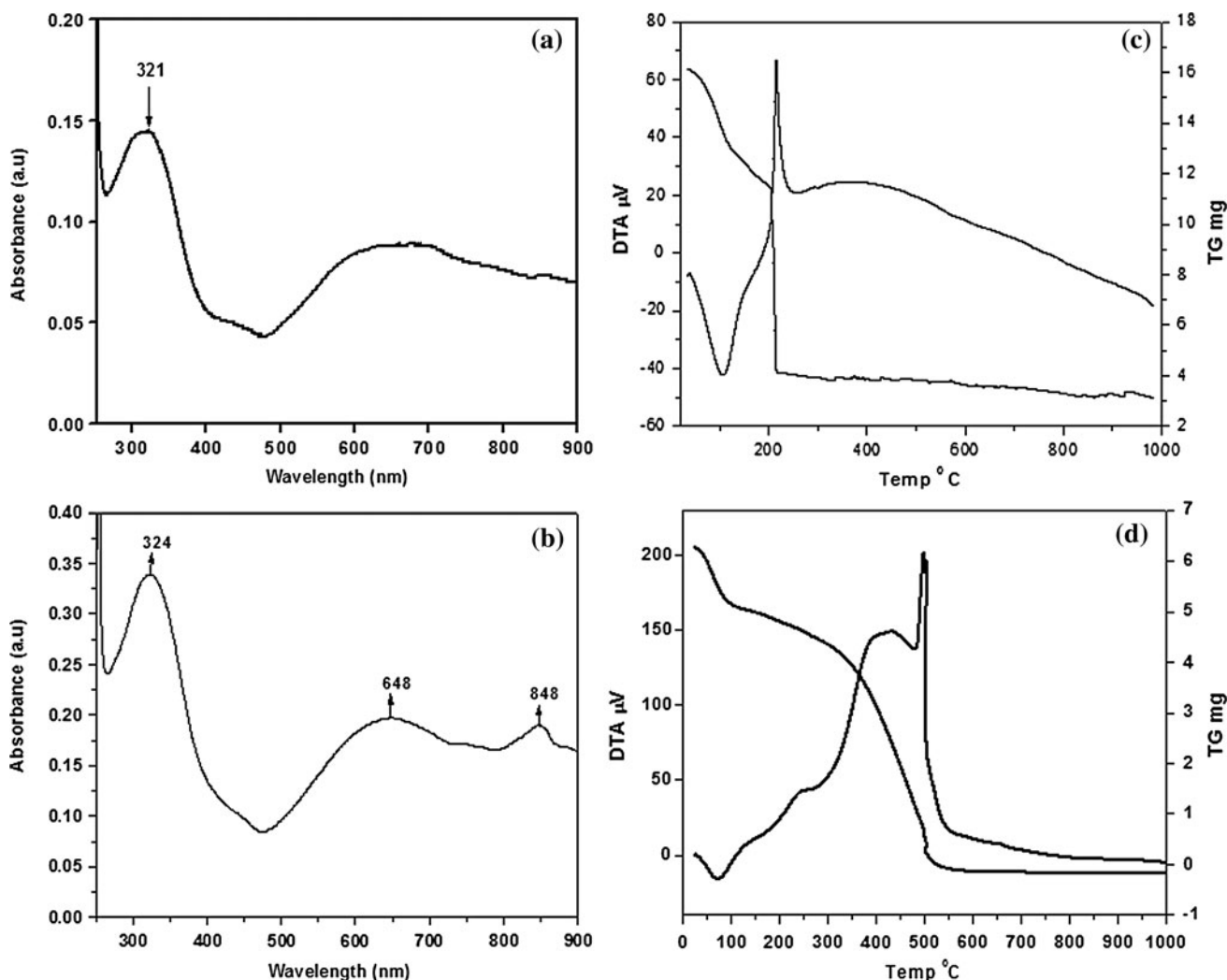

Fig. 2 UV–Vis spectra of **a** CeO_2 nanoparticles, **b** PANI/CeO_2 nanocomposites and TG/DTA thermogram of **c** CeO_2 nanoparticles, and **d** PANI/CeO_2 nanocomposites

of different phases (conducting and insulating) of the resulting PANI/CeO$_2$ nanocomposites.

Thermal analysis

The thermogravimetric and differential thermal analyses (TG/DTA) are important to check the thermal stability and to identify various transitions (exothermic and endothermic) of a substance. Figure 2c shows the TG/DTA curves of as-prepared CeO$_2$ nanoparticles. The weight loss indicates the decomposition of hydrated oxide, i.e., CeO$_2$·H$_2$O to CeO$_2$. The amount of weight loss was low, which suggests that the samples consisted of a mixture of more CeO$_2$ than the hydrated ceria, also attributed to the low hygroscopic nature of CeO$_2$ [42, 43]. Three major weight losses are seen. The poorly resolved first step accounted for 2.74 mg weight loss up to 102.4 °C due to dehydration of the hydrated CeO$_2$, which produced an endothermic peak. In the second step, weight loss was about 1.76 mg, and an exothermic peak is seen at 214.88 °C. This exothermic peak also corresponds to the dehydration of CeO$_2$ and the oxidation of Ce^{3+} [44]. Further increase in temperature beyond 225 °C also triggered the decomposition of the anhydrous salt, contributing to the third step of weight loss. The third step accounts for weight loss due to the decomposition of residual nitrate.

In the case of PANI/CeO$_2$ nanocomposite, the complete process of weight loss is composed of three stages (Fig. 2d), namely, the dehydration from PANI and CeO$_2$, decomposition of aniline oligomers and/or dehydration of water in the crystallization of CeO$_2$ nanoparticles, decomposition of anions in CeO$_2$ and decomposition of PANI/CeO$_2$ nanocomposite. The percentage of weight loss in PANI/CeO$_2$ nanocomposite is higher than the pristine PANI. In PANI/CeO$_2$ nanocomposite (Fig. 2d), the three step weight loss (I: 35–95 °C, II: 165–305 °C, and III: 355–505 °C) process is quite different from the thermal behavior of PANI. In PANI/CeO$_2$ nanocomposite, the DTA has six endothermic peaks at 70, 175, 265, and 478 °C. Rosenheim's dehydration experiment [45] showed that, during the crystallization of polyoxometalates, water was easily expelled from crystals at moderate temperatures, but the appropriate number of constitutional water molecules were expelled only at much higher temperatures accompanied by the disintegration of the PANI/CeO$_2$ nanocomposite [46]. The results showed that the thermal decomposition temperature of PANI/CeO$_2$ nanocomposite was 505 °C, which was lower than that of control PANI (552 °C). The drop of temperature was associated with the influence of CeO$_2$ nanoparticles upon PANI macromolecules. An interaction between CeO$_2$ nanoparticles and PANI probably weakened the interaction of inter-chains in PANI macromolecule, and helped in the degradation of the

skeletal structure of PANI chains [47]. Here, the data indicate that the improvement trend of the degradation curve for PANI/CeO$_2$ nanocomposite was confirmed due to the capping of CeO$_2$ nanoparticles within the sulfonated PANI matrix.

SEM and HRTEM analysis

From SEM and HRTEM images of CeO$_2$ nanoparticles, the morphology of nanoparticles is observed to be spherical shaped particles with slight agglomeration. The images indicate that the nanoparticles were nearly spherical and slightly elongated and it confirms the possibility of different crystallographic planes of different atomic density. The HRTEM images demonstrate that the nanoparticles range from 10 to 20 nm, which are approximately the sizes reported by Chen and Chang [48]. These images also provide evidence for the formation of larger aggregates (supra-aggregates) as observed in the HRTEM image which is shown in Fig. 3c. These supra-aggregates are likely the stable form of these nanoparticle suspensions. We could also observe some smaller particles of 5–6 nm in size, which are combined together to grow to the irregular particle with the size about 20 nm like a single particle observed by HRTEM [49]. As the CeO$_2$ particles tend to lower the surface energy, we could observe the agglomeration of nanoparticles like spherical shape with the size between 20 and 60 nm in the SEM image. SEM and HRTEM images of PANI/CeO$_2$ nanocomposites are presented in Fig. 3b and d. It is noticed that the images show a uniform view of the CeO$_2$ nanoparticle-capped PANI cages of PANI/CeO$_2$ nanocomposite. The particles were spherical and granular in nature and seemed to be nanosized, typically in the range of <50 nm. It can be seen that PANI nanoparticles have a typical size range of several to tens of micrometers structure, which transformed to PANI/CeO$_2$ nanocomposite particles after in situ polymerization reaction. This indicates that CeO$_2$ nanoparticles have a nucleus effect and caused a homogeneous PANI core shell type morphology with relatively uniform diameter of about 20 nm. The CeO$_2$ nanoparticles would be present not only on the nanocomposite surface but also distributed through their interior. The tendency to cluster formation could also be noted. It can be thought that there are also free CeO$_2$ particles in colloid dispersions with a small size. In Fig. 3b, clusters of PANI/CeO$_2$ nanocomposite are clearly observed, and in higher magnification the net like structure of PANI was seen obviously. According to the SEM images, it was considered that the nanostructured CeO$_2$ nanoparticles embedded within the net like structure built by PANI chains. It implies that the nanocomposite is able to increase the liquid–solid interfacial area, provides a path for the insertion and extraction of ions, and ensures a high

reaction rate. The results obtained in this study are found to be in agreement with the study obtained by other researchers [50–53].

HRTEM image of the PANI/CeO$_2$ core–shell nano-composite image (fig. 3d) indicates that the CeO$_2$ nanoparticles are embedded in the PANI matrix forming the core–shell structure. The black core is CeO$_2$ with the

diameter in the range of 15–20 nm, and the light colored shell is PANI in the nanocomposite, due to the different electron penetrability. From Fig. 3d, it is clearly observed that the polymer matrix is coated or glued on to the surface of the granular CeO$_2$, the dark shaded inner part (core) and the PANI layers of different thickness act as the outer coated surface (shell, light shaded) of CeO$_2$ nanoparticles.

Fig. 3 SEM image of **a** CeO$_2$ nanoparticles, **b** PANI/CeO$_2$ nanocomposite, **c** HRTEM image of CeO$_2$ nanoparticles, **d** PANI/CeO$_2$ nanocomposite, **e** SAED pattern of PANI/CeO$_2$ nanocomposite, and **f** CeO$_2$ nanoparticles
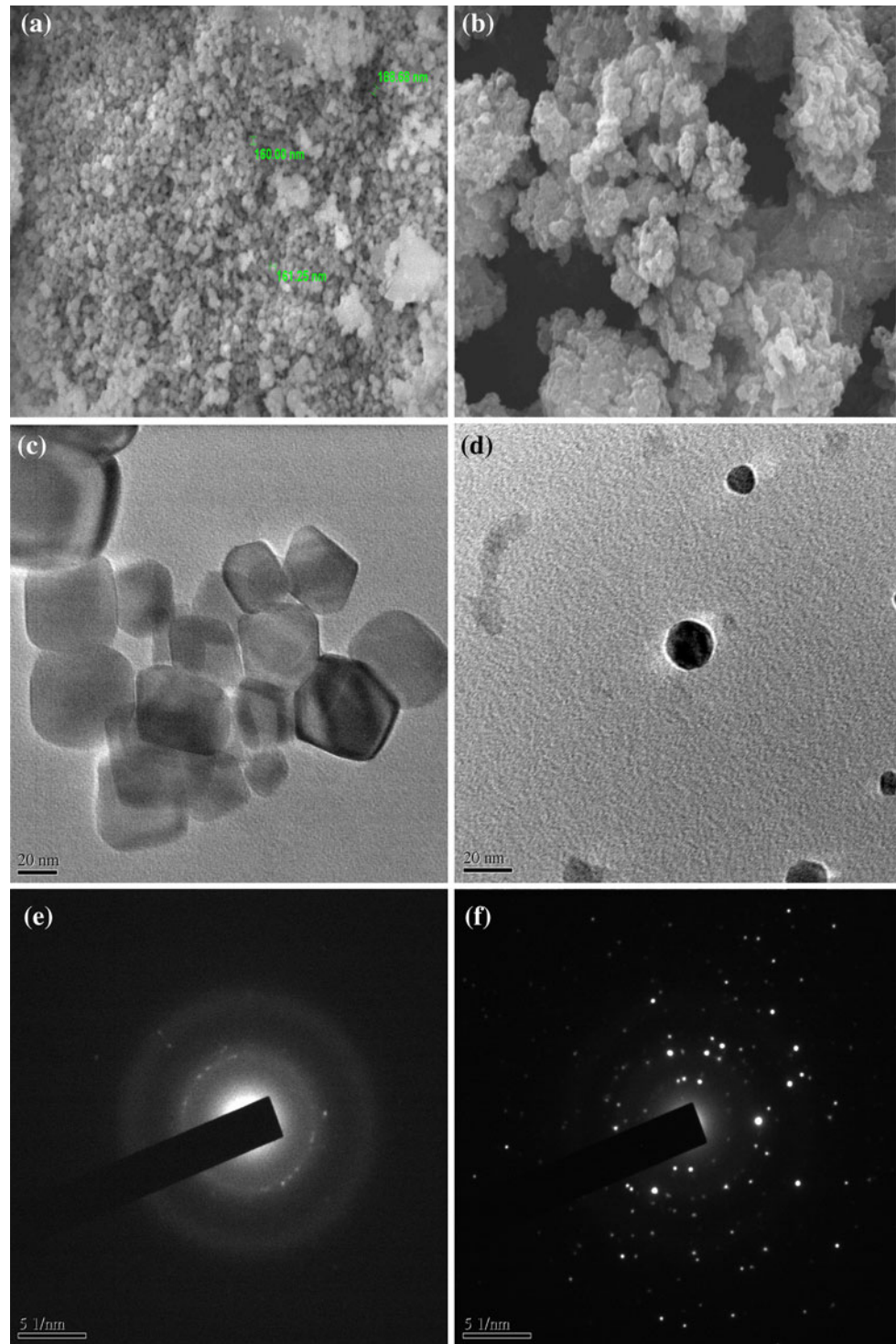
It is indicated that the nanocomposite is composed of CeO_2 nanoparticles and PANI, which is in accordance with the results obtained by XRD analysis. The selected area electron diffraction (SAED) pattern of CeO_2 nanoparticle is shown in Fig. 3f. The high crystallinity of the powder leads to its corresponding well-pronounced Debye–Scherrer diffraction rings in the SAED pattern that can be assigned to the reflections (1 1 1), (2 0 0), (2 2 0), and (3 1 1) of cubic phase of CeO_2. There are no additional rings in the SAED pattern stemming from any crystalline impurities. To get further insight into the atomic order of the CeO_2 nanoparticles, high-resolution images were recorded. To obtain a particle size distribution from transmission electron micrographs we manually measured the particle sizes for 50 particles to ensure a reliable representation of the actual size distribution. The crystallite size is about 10–20 nm as estimated from the TEM micrographs. The experimental and calculated XRD patterns provide a volume-weighed average grain size of 19.9 nm, which is in good agreement with the particle size observable on the TEM image. The interplanar spacing of the CeO_2 nanoparticles is about 0.31 nm, which is identical with the (1 1 1) facet distance of bulk CeO_2 phase. They appear to be single crystals domain and exhibit 0.19 or 0.31 nm *d*-spacing for (2 2 0) and (1 1 1) reflections. The *d*-spacing of four rings in Fig. 3f are 0.312, 0.271, 0.191, 0.163 nm, which are consistent with reflections (1 1 1), (2 0 0), (2 2 0), and (3 1 1) of cubic structure of CeO_2 (PCPDF 34-0394). The SAED pattern of PANI/CeO_2 nanocomposite is shown in Fig. 3e. The high crystallinity of the powder leads to its corresponding well-pronounced Debye–Scherrer diffraction rings in the SAED pattern that can be assigned to the reflections (2 0 0), (2 2 0), and (3 1 1) of cubic phase of PANI/CeO_2 nanocomposite.

Conclusion

The nanomaterials like pure CeO_2 nanoparticles and PANI/CeO_2 nanocomposite have been synthesized by microwave-assisted solution method and they were characterized by various studies. XRD patterns showed that the obtained CeO_2 nanoparticles were of cubic phase. The blue-shift phenomenon of the UV absorption threshold has been found and this is attributed to the size quantization effect. The morphological and structural studies of the synthesized particles were found by SEM, TEM, HRTEM, and SAED studies. The HRTEM of the images indicate that the CeO_2 nanoparticles were embedded in the PANI matrix forming the core–shell structure. The thermal stability of the samples was studied by TG/DTA analysis. The functional groups of the samples were identified from FT-IR spectra. The synthesized PANI/CeO_2 nanocomposite can be used for fabrication of films or coatings, or even in further polymer blending.

References

1. Malinauskas A (2001) Polymer 42:3959
2. Skotheim TA, Elsenbaumer RL, Reynolds JR (1998) Handbook of conducting polymers. Dekker, New York
3. Werne TV, Patten TE (2001) J Am Chem Soc 123:7497
4. Zhang H, Ruhe J (2005) J Macromol 38:10743
5. Sandra L, Narae K, Nathan D (2006) Chem Mater 18:5137
6. Pethkar S, Patil R, Kher J, Vijayarnohanan K (1999) Thin Solid Films 349:105
7. Khanna PK, Singh N, Charan S, Sunil Lonkar P, Satyanarayana Reddy A, Patil Y, Kasi Viswanath A (2006) Mater Chem Phys 97:288
8. Hesheng X, Qi W (2002) Chem Mater 14:2158
9. Danielle C, Michelle S, Ivo A, Aldo Z (2003) Chem Mater 15:4658
10. Bondioli F, Bonamartini A, Leonelli C, Manfredini T (1999) Mater Res Bull 34:2159
11. Bo K, Jae J, Seung H, Jinsoo J (2002) Macromolecules 35:1419
12. Park J, Park S, Koukitu A, Hatozaki O, Oyarna N (2004) Synth Met 141:265
13. Sui X, Chu Y, Xing S, Liu C (2004) Mater Lett 58:1255
14. Wu NC, Shi EW, Zheng YQ, Li WJ (2002) J Am Ceram Soc 85:2462
15. Hirano M, Kato E (1996) J Mater Sci Lett 15:1249
16. Sanchez MG, Gazquez JL (1987) J Catal 104:120
17. Jiang M, Wood NO, Komanduri R (1998) Wear 220:59
18. Izu N, Shin W, Murayarna N, Kanzaki S (2002) Sens Actuators B 87:95
19. Yabe S, sato T (2003) J Solid State Chem 171:7
20. Chen PL, Chen IW (1993) J Am Ceram Soc 76:1577
21. Djuricic B, Pickering S, Euro J (1999) Ceram Soc 19:1925
22. Zhou XD, Huebner W, Anderson HU (2002) Appl Phys Lett 80:3814
23. Li LP, Lin XM, Li GS, Inomata H (2001) J Mater Res 16:3207
24. Komarneni S, Rajha R (1999) Mater Chem Phys 61:50
25. Yang H, Huang C, Tang A, Zhang X, Yang W (2005) Mater Res Bull 40:1690
26. Yu K-L, Ruan G-L, Ben Y-H, Zou J-J (2007) Mater Sci Eng B 139:197
27. Chang H-Y, Chen H-I (2005) J Cryst Growth 283:457
28. Jiaoxing X, Li G, Li L (2008) Mater Res Bull 43:990
29. Jin H, Wang N, Liang X, Hou S (2010) Mater Lett 64:1254
30. Brightson M, Selvarajan P, Kennady Vethanathan J, Freeda TH, Meenakshi Sundar S (2010) Recent Res Sci Technol 2(6):29
31. Abdiryim T, Xiao-Gang Z, Jamal R (2005) Mater Chem Phys 90:367
32. Goel S, Gupta A, Singh KP, Hehrotra R, Kandpal HC (2007) Mater Sci Eng A 443:71
33. Feng W, Sun E, Fujii A, Wu HC, Niihara K, Yoshino K (2000) Bull Chem Soc Jpn 73:2627
34. Li X, Chen W, Bian C, He J, Ning X, Xue G (2003) Appl Surf Sci 16:217

35. Zhang DS, Fu HX, Shi LY, Pan CS, Li Q, Chu YL, Yu WY (2007) Inorg Chem 46:2446
36. Phoka S, Laokul P, Swatsitang E, Promarak V, Seraphin S, Maensiri S (2009) Mater Chem Phys 115:423
37. Nakagawa K, Murata Y, Kishida M, Adachi M, Hiro M, Susa K (2007) Mater Chem Phys 104:30
38. Chuang F-Y, Yang S-M (2008) J Colloid Interface Sci 20:194
39. Tao Y, Wang H, Xia Y, Zhang G, Haiping W, Tao G (2010) Mater Chem Phys 124:541
40. Karatchevtseva I, Zhang Z, Hanna J, Luca V (2006) Chem Mater 18:4908
41. Kulkarni M, Viswanath A (2004) J Macromol Sci Part A 41:1173
42. Kamruddin M, Ajikumar PK, Nithya R, Mangamma G, Tyagi AK, Raj B (2006) Powder Technol 161:145
43. Kamruddin M, Ajikumar PK, Nithya R, Tyagi AK, Raj B (2004) Scr Mater 50:417
44. Djuricic B, Pickering S (1999) J Eur Ceram Soc 19:1925
45. Rosenheim A, Schwer H (1914) Z Anorg Chem 89:224
46. Baker LCW, Glick DC (1998) Chem Rev 98:3
47. Li XW, Chen W, Bian CQ, He JB, Xu N, Xue G (2003) Appl Surf Sci 217:16
48. Chen HI, Chang HY (2004) Colloids Surf A 242:61
49. Hu CG, Zhang ZW, Liu H, Gao PX, Wang ZL (2006) Nanotechnology 7:5983
50. Phang SW, Tadokoro M, Watanabe J, Kuramoto N (2008) Curr Appl Phys 8:391
51. Jing S, Xing S, Lianxiang Y, Yan W, Zhao C (2007) Mater Lett 61:2794
52. Mo T-C, Wang H-W, Chen S-Y, Yeh Y-C (2008) Ceram Int 34:1767
53. Jiang J, Ai L, Li L (2009) J Non-Cryst Solids 355:1733